



ELSEVIER

Catalysis Today 38 (1997) 13–22

CATALYSIS
TODAY

Modelling the dynamics of the N₂O reduction on iron oxide

Harvey Randall, Ralf Doepper, Albert Renken*

Institute of Chemical Engineering, Swiss Federal Institute of Technology, CH-1015 Lausanne, Switzerland

Abstract

The reduction of N₂O to N₂ on iron oxide under transient conditions was studied in the temperature range of 270–340°C. Six different models were used to simulate the experimental data. The conventional second-order reaction between gas phase N₂O and surface oxygen vacancies failed to describe the dynamic experiments. Upon introducing linear or exponential distributions of the second-order surface reaction rate constant in function of the degree of reduction of the surface, satisfactory fittings to the experiment could not be achieved either. It was necessary to take into account subsurface oxygen diffusion to describe the low rates of reaction measured at low degrees of reduction of the catalyst. The combination of subsurface oxygen diffusion with a linear activity distribution for the surface reaction provided a good description of the transient N₂O reduction. Finally, the surface reaction rate constant as well as the diffusion coefficient of oxygen in iron oxide could be fitted with the Arrhenius law.

Keywords: Transient kinetics; Oxide catalysts; Oxygen diffusion

1. Introduction

The reduction of N₂O to N₂ was here investigated within the framework of the reduction of NO with CO on Fe₂O₃/SiO₂, since nitrous oxide is the intermediate product on the reaction pathway towards nitrogen. In a previous work [1], we have studied the reduction of N₂O on silica-supported iron oxide in a fixed-bed tubular reactor under transient conditions. It was shown that on reduced catalysts (Fe₃O₄), nitrous oxide is converted to nitrogen even in the absence of CO. The qualitative analysis of the transient responses lead to the conclusion that the reaction follows an Eley–Rideal mechanism, according to which N₂O reacts with surface oxygen vacancies (symbolised by ()),

thereby leading to the formation of N₂ and surface oxygen (symbolised by (O)) (Eq. (1)).



During this process, the catalyst is reoxidised to Fe₂O₃. At high oxidation states of the catalyst, the rate of its reoxidation became very low, so that long times were required to fully reoxidise the iron oxide (up to an hour). The slowness of this process did not result from pore diffusion limitations, as shown by experiments using different particle size [1]. Once the catalyst has been totally oxidised, the reaction stops, indicating that the decomposition of N₂O into N₂ and O₂ does not occur in the temperature range of concern, i.e., 250–340°C. It is then necessary to reduce the catalyst again (CO or H₂) in order to restore its activity for the N₂O reduction. Nitrogen mass balance considerations allowed us to conclude that no significant

*Corresponding author. Tel.: (41-21) 693-3181; Fax: (41-21) 693-3190; e-mail: renken@igcsun3.epfl.ch

amount of nitrogen containing species were adsorbed on the catalyst surface, which confirms the reaction step described in Eq. (1). The aim of this work is to establish a model for the quantitative description of this transient behaviour. Effects such as subsurface oxygen diffusion as well as linear and exponential activity distributions were taken into account for the modelling of the dynamic experiments.

2. Experimental

The reaction was carried out in a glass fixed-bed tubular reactor (internal diameter: 5 mm, length: 300 mm). The catalyst used in this study consisted of 200–250 µm particles of silica-supported Fe₂O₃, prepared by iron nitrate impregnation. The amount of Fe, as determined by plasma emission, is 10.4 mass% Fe. Such a catalyst has a specific area of 252 m²/g and a mean pore diameter of 11.3 nm. Prior to transient experiments, the catalyst was fully reduced to Fe₃O₄ with either CO or H₂, which were then desorbed at 430°C in an Ar flow. Dynamic experiments consisted in step changes of N₂O inlet mole fraction (from 0 to $y_{N_2O,0}$) on reduced catalysts, which were performed by substituting, with the help of a four-way valve, an Ar flow at the inlet of the reactor with an N₂O/Ar flow at same pressure and total flow rate. During these concentration steps, the pressure disturbance never exceeded 0.5 kPa. Step response experiments were conducted at different temperatures, using two different total flow rates and two feed concentrations of N₂O, as can be seen in Table 1. A more detailed description of the apparatus and experimental procedures is given elsewhere [1].

The value for the axial Peclet number in the fixed bed was estimated to be $Pe_{ax}=2$ [2]. The length of the reactor (L) was 0.01 m, and the particle diameter (d_p) was taken as 2.25×10^{-3} m. From these values, a Bodenstein number ($Bo=Pe_{ax}L/d_p$) in the fixed bed of approximately 90 was calculated. With such a high value for Bo , the fixed bed can be considered as a plug flow reactor [2]. The inlet function ($y_{N_2O,0}(t)$) after switching the inlet flow from pure Ar to N₂O/Ar appeared to significantly differ from the ideal square function, due to axial dispersion in the tubing between the four-way valve and the reactor. Therefore, the inlet function $y_{N_2O,0}(t)$ was measured for the different flow

Table 1
Experimental operating conditions

Run	$y_{N_2O,0}$ ($\times 10^3$)	T (°C)	Q (ml(NTP)/min)	m_{cat} ($\times 10^5$ kg)
1	2.0	290	200	6.77
2	2.0	310	200	6.77
3	2.0	340	200	6.77
4	3.9	290	200	7.90
5	4.0	310	200	7.90
6	4.0	340	200	7.90
7	4.3	274	100	6.77
8	4.0	290	100	6.77
9	4.0	310	100	6.77
10	4.1	324	100	6.77
11	4.1	340	100	6.77

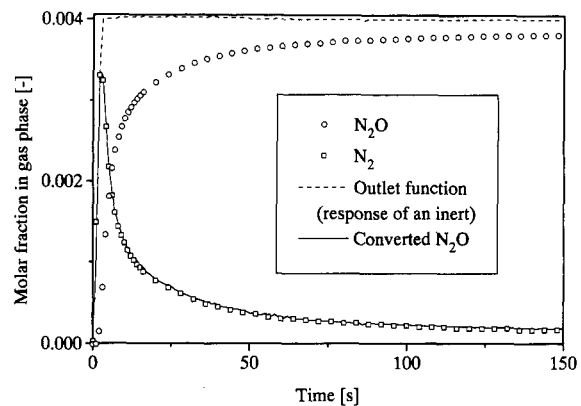


Fig. 1. Typical transient response to a concentration step of N₂O on a reduced catalyst. Conditions: $y_{N_2O,0}=0.004$, $T=310^\circ\text{C}$, $Q=200 \text{ ml(NTP)/min}$ (run 5). Some data points were omitted for clarity of the graph.

rates and N₂O feed concentrations used in runs 1–11, and was used for modelling (Eq. (14)) as boundary condition for N₂O concentration at the reactor inlet.

Fig. 1 shows the typical transient response of a reduced catalyst (Fe₃O₄) to a concentration step of N₂O from 0 to 0.004 (run 5). The main qualitative features of the dynamic experiments appear in this figure, where the transient responses of N₂O and N₂ are compared to the response of the reactor to an inert tracer (He) with an inlet molar fraction of 0.004 (outlet function). The initial rate of reaction is very fast, so that at the beginning of the transient, the response of reaction product nitrogen is superimposed to the response of He. During this period, N₂O is totally

converted. After approximately 30 s, the reduction rate of N₂O falls to very low values, but the formation of N₂ is still observed for over 30 min. The amount of converted N₂O, calculated by subtracting the response of N₂O to the response of the inert tracer, is superimposed to the response of nitrogen, indicating that the nitrogen mass balance is always respected. Therefore, no adsorption of nitrous oxide needs to be taken into account for modelling.

3. Model equations

3.1. Kinetic models

In this section, three different kinetic models are presented, which were used for modelling the dynamic experiments.

3.1.1. Second-order surface reaction

The rate (r) of the surface reduction of N₂O (Eq. (1)) was expressed with the following second-order equation:

$$r = kc_{\text{N}_2\text{O}}\phi_s, \quad (2)$$

where ϕ_s is the degree of reduction of iron oxide at the surface ($\phi_s = c_{(\text{N}_2\text{O})s}/N_s$, where N_s is the total concentration of sites).

3.1.2. Second-order surface reaction with a linear activity distribution

The following activity distribution was introduced, assuming a linear decay of the rate constant with the degree of reduction of the catalyst

$$k = k_r\phi_s, \quad (3)$$

where k_r is the rate constant for the reduced catalyst ($\phi_s = 1$).

The rate equation becomes

$$r = k_rc_{\text{N}_2\text{O}}\phi_s^2. \quad (4)$$

3.1.3. Second-order surface reaction with an exponential activity distribution

By analogy with the Brunauer, Love and Keenan equation for the adsorption rate constant on non-ideal surfaces [3], which is an exponential relation between the adsorption rate constant and the concentration of

free sites, the following activity distribution was introduced, assuming an exponential decay of the rate constant with the degree of reduction of the catalyst

$$k = \beta(e^{\alpha\phi_s} - 1). \quad (5)$$

When the surface of the catalyst is reduced ($\phi_s = 1$), k becomes

$$k = k_r = \beta(e^\alpha - 1), \quad (6)$$

where k_r is the rate constant for the reduced catalyst.

The constant β is therefore

$$\beta = \frac{k_r}{e^\alpha - 1} \quad (7)$$

and k becomes

$$k = \frac{k_r}{e^\alpha - 1}(e^{\alpha\phi_s} - 1). \quad (8)$$

At last, the following rate expression is obtained:

$$r = \frac{k_r}{e^\alpha - 1}(e^{\alpha\phi_s} - 1)\phi_s c_{\text{N}_2\text{O}}. \quad (9)$$

3.2. Mass balance equations

As shown in Fig. 1, at the beginning of the dynamic experiment, the conversion of N₂O reaches high values (100% in the first seconds). This gives rise to an important concentration gradient of N₂O and N₂ in the axial direction of the fixed bed. Therefore, the reactor cannot be taken as a differential (gradientless) reactor, but has to be treated as an integral reactor.

3.2.1. Mass balance for gas phase species in a non-stationary tubular plug flow reactor

The mass balance equation for a gas phase species j (N₂O or N₂) is given by the expression

$$\frac{\partial c_j}{\partial t} = -\frac{1}{\tau} \frac{\partial c_j}{\partial x} + R_j \rho_{\text{cat}} \frac{1 - \epsilon_b}{\epsilon_b}. \quad (10)$$

Variables and parameters are defined in Section 6.

The space time τ (referred to gas volume) in Eq. (10) is

$$\tau = \frac{1}{Q} \frac{\epsilon_b}{1 - \epsilon_b} \frac{m_{\text{cat}}}{\rho_{\text{cat}}}. \quad (11)$$

The rate R_j in Eq. (10) is given by

$$R_{\text{N}_2} = -R_{\text{N}_2\text{O}} = r. \quad (12)$$

The concentration of a component j in the gas phase c_j is converted to the molar fraction in the gas phase y_j via the ideal gas law.

For an N_2O concentration step from 0 to $y_{\text{N}_2\text{O},0}$ at $t=0$, the initial condition for gas phase species (N_2O or N_2) is

$$c_j(x, 0) = 0 \quad (13)$$

and the boundary conditions at the reactor inlet ($x=0$) are given by

$$c_{\text{N}_2\text{O}}(0, t) = \frac{p}{RT} y_{\text{N}_2\text{O},0}(t), \quad c_{\text{N}_2}(0, t) = 0. \quad (14)$$

By solving Eq. (10), the concentration gradient of the gas phase species in the axial direction of the reactor (x) can be obtained. However, the rate of formation of gas phase species R_j is a function of the degree of reduction of the catalyst at the surface ϕ_s , as shown in Section 3.1. Eq. (10), therefore, has to be solved simultaneously with the mass balance equation for ϕ_s .

3.2.2. Mass balance for ϕ with subsurface oxygen diffusion

Subsurface oxygen diffusion was used in this work to account for the long tailing of the N_2O and N_2 responses during the experimental transients. Thus, an additional dimension has to be introduced: the distance into the iron oxide layer (z), in which oxygen diffusion takes place. The reduction of N_2O at the surface of the catalyst ($z=1$) produces surface oxygen which diffuses into subsurface oxygen vacancies, giving rise to a concentration profile of the degree of reduction of iron oxide ($\phi=c_{\text{O}_2}/N_s$, where N_s is the total concentration of sites) as a function of z . Furthermore, since the rate (r) of the surface reaction is a function of the concentration of N_2O , the N_2O concentration profile in the x -direction gives rise to a ϕ -profile as a function of x . The degree of reduction of the iron oxide is, therefore, a function of x , z and t .

For spherical iron oxide crystallites, the dimensionless mass balance equation for the degree of reduction of the iron oxide at the surface ($z=1$, where $\phi=\phi_s$) is

$$\frac{\partial \phi_s}{\partial t}(x, z=1, t) = \frac{1}{t_d} \left(\frac{\partial^2 \phi}{\partial z^2} + 2 \frac{\partial \phi}{\partial z} \right)_{z=1} + \frac{R_\phi}{N_s}. \quad (15)$$

The characteristic diffusion time of oxygen into the iron oxide layer t_d is given by

$$t_d = \frac{\delta^2}{D}. \quad (16)$$

The rate R_ϕ of Eq. (15) is given by

$$R_\phi = -r. \quad (17)$$

In the bulk of the iron oxide layer ($z < 1$), where no reaction occurs

$$\frac{\partial \phi}{\partial t}(x, z < 1, t) = \frac{1}{t_d} \left(\frac{\partial^2 \phi}{\partial z^2} + \frac{2}{z} \frac{\partial \phi}{\partial z} \right). \quad (18)$$

For a totally reduced catalyst, the initial condition for Eqs. (15) and (18) is

$$\phi(x, z, 0) = 1. \quad (19)$$

The iron oxide crystallites on the surface of the silica support can be considered symmetrical around their centreplanes. Therefore, the boundary condition at the centre ($z=0$) of the particle is

$$\frac{\partial \phi}{\partial z}(x, 0, t) = 0. \quad (20)$$

Finally, six different models, described in Table 2, were built up by combining the mass balance equations (Eqs. (10),(15) and (18)) with the reaction rates of Eqs. (2),(4) and (9). In models 1–3, only the surface reaction (Eq. (1)) was taken into account, by using the rate equations in Eqs. (2),(4) and (9), respectively, for models 1, 2 and 3. For models 1–3, subsurface oxygen diffusion was disregarded by setting $1/t_d$ equal to zero in Eqs. (15) and (18). In models 4, 5 and 6, the surface reaction was described, respectively, with the rate equations in Eqs. (2),(4) and (9), and subsurface oxygen diffusion was taken into account for each of these three models. The system of partial differential equations in Eqs. (10),(15) and (18) was solved using the finite difference approximation method, using nine nodes in the x -direction and 40 nodes in the z -direction. Numerical integration was carried out using a variable step algorithm (Gear) [4]. Optimisation of parameters t_d , k , k_r and α was performed by fitting the calculated molar fractions of N_2 and N_2O at the outlet of the reactor to their experimental values, using the Nelder–Mead search algorithm and the likelihood function as objective function [4]. In addition to N_2 and N_2O molar fractions, numerical integration also

Table 2
Description of models

Model	Subsurface oxygen diffusion	Reverse characteristic diffusion time ($1/t_d$)	Activity distribution	Rate constant of surface reaction (k)
1	None	0	None	k
2	None	0	Linear	$k_r\phi$
3	None	0	Exponential	$\frac{k_r}{e^\alpha - 1} (e^{\alpha\phi} - 1)$
4	Taken into account	>0	None	k
5	Taken into account	>0	Linear	$k_r\phi$
6	Taken into account	>0	Exponential	$\frac{k_r}{e^\alpha - 1} (e^{\alpha\phi} - 1)$

provides the degree of reduction of the catalyst, ϕ , as a function of time and reactor length (x) for all models. For models 4 and 5, ϕ is also calculated as a function of position in the oxide layer (z). ϕ is merely a calculated variable, inherent to the different models, since it was not measured experimentally during this work.

4. Experimental results and modelling

4.1. Model discrimination

In Fig. 2, the experimental transient response of N_2 to a concentration step of N_2O with a molar fraction of 0.002 in the feed (run 2) is compared to the responses calculated using models 1–6 with optimum parameter values. Models 1 and 2, which do not take subsurface oxygen diffusion into account, obviously fail to describe the transient behaviour. Model 3, though better than models 1 and 2, is unable to accurately describe the high initial reaction rate as well as the significant decrease in reaction rate at higher oxidation states of the catalyst. The description of the transient response is significantly improved by introducing subsurface oxygen diffusion (models 4–6). The best fitting to experimental data was obtained by combining subsurface oxygen diffusion to an exponential activity distribution (model 6). Model 6 also provided good fittings to the experimental data for all the other runs. However, the parameters of model 6 (α , k_r and t_d) were found to be quite strongly related, so that it was not possible to determine them on the basis of our experiments. Due to this relation between the parameters, neither k_r nor $1/t_d$ follow an Arrhenius behaviour. Consequently, model 6 does not have any

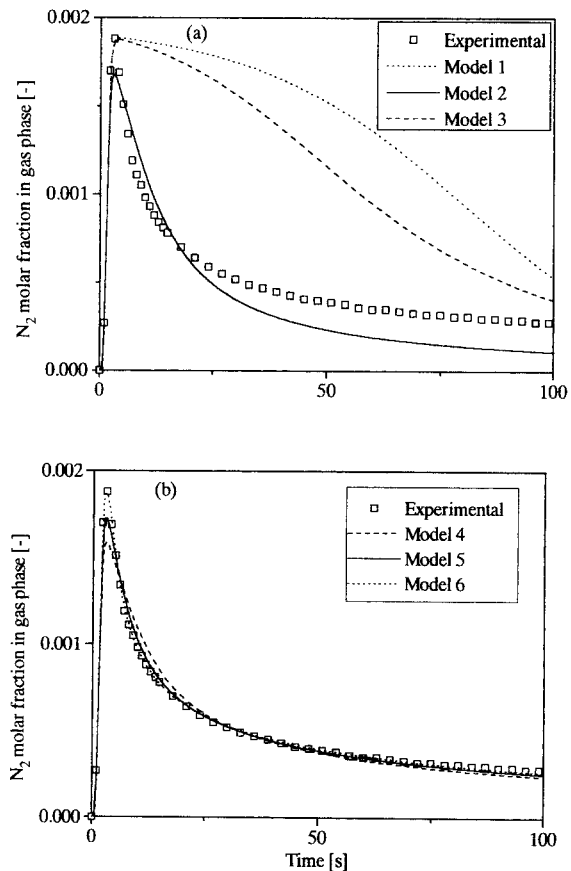


Fig. 2. N_2 response to a N_2O concentration step on a reduced catalyst. Comparison between experimental data and models 1–6. Conditions: $y_{N_2O,0}=0.002$, $Q=200$ ml (NTP)/min, $T=310^\circ\text{C}$ (run 2). Some data points were omitted for clarity of the graph.

predictive power. The remarks concerning model 6 mentioned above lead us to disregard model 6 in favour to model 5, which provides only slightly poorer fittings to experimental data. Model 5, in addition,

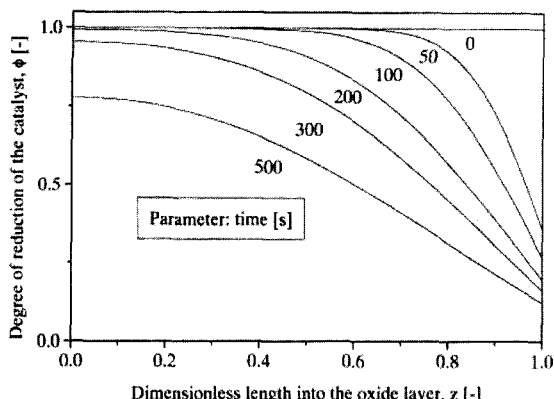


Fig. 3. Calculated (model 5) spatio-temporal behaviour of ϕ for a N_2O concentration step on a reduced catalyst. Conditions: $y_{N_2O,0}=0.002$, $Q=200$ ml(NTP)/min, $T=310^\circ\text{C}$ (run 2). Catalyst surface: $z=1$. Centre of particle: $z=0$.

contains only two parameters, which both follow the Arrhenius law, as will be shown in Section 4.2. Model 5 has, therefore, contrary to model 6, a predictive power.

The spatio-temporal behaviour of the degree of reduction of iron oxide ϕ calculated with model 5 is depicted in Fig. 3. In this figure, the calculated ϕ -profile in the iron oxide layer in the middle of the fixed bed ($x=0.5$) is given for different reaction times. The degree of reduction of the surface ($z=1$) rapidly decreases during the first seconds due to the fast consumption of surface oxygen vacancies by N_2O , combined with the linear decay of the rate constant k with decreasing ϕ . Thereafter, the diminution of ϕ is slower, due to the limitation of the process by subsurface oxygen diffusion, and the ϕ -profile becomes more uniform.

Fig. 4 shows the experimental and calculated (model 5) responses of N_2O and N_2 to concentration steps of N_2O with a molar fraction of 0.002 in the feed, at three different temperatures (290°C , 310°C and 340°C), at a total flow rate of 200 ml(NTP)/min (runs 1–3). A good description of the transients is obtained at each temperature. Good fittings to the experimental data were also provided by model 5 at a higher N_2O inlet molar fraction (runs 4–6, with $y_{N_2O,0} = 0.004$) (Fig. 5), and with a lower total flow rate (runs 7, 9 and 11, with $Q=100$ ml(NTP)/min) (Fig. 6). The initial rate constant k_r and the reverse characteristic diffusion time $1/t_d$ follow an Arrhenius dependence, as can be

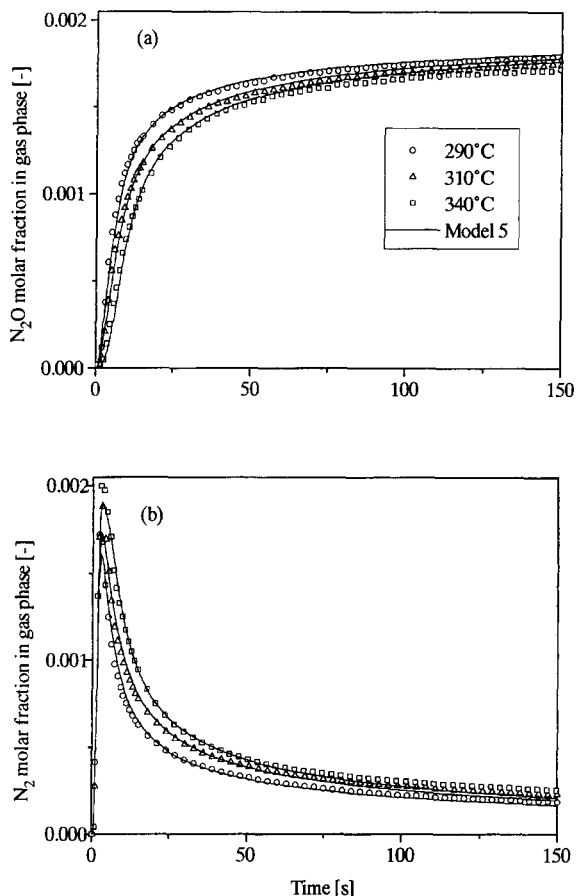


Fig. 4. Comparison between model 5 and experiment for a N_2O concentration step on a reduced catalyst at different temperatures. Conditions: $y_{N_2O,0}=0.002$, $Q=200$ ml(NTP)/min (runs 1–3). Some data points were omitted for clarity of the graph.

seen in Fig. 7, where the logarithms of their optimum values obtained for runs 1–11 are plotted versus reciprocal temperature. The activation energies for reaction and subsurface oxygen diffusion (respectively E_r and E_d) and the corresponding pre-exponential factors k_{r0} and $1/t_{d0}$ are given in Table 3.

Table 3
Parameters for model 5

E_r (kJ/mol)	72 ± 7
E_d (kJ/mol)	47 ± 6
k_{r0} ($\text{m}^3/\text{kg}_{\text{cat}} \text{s}$)	7.6×10^5
$1/t_{d0}$ (s^{-1})	2.6

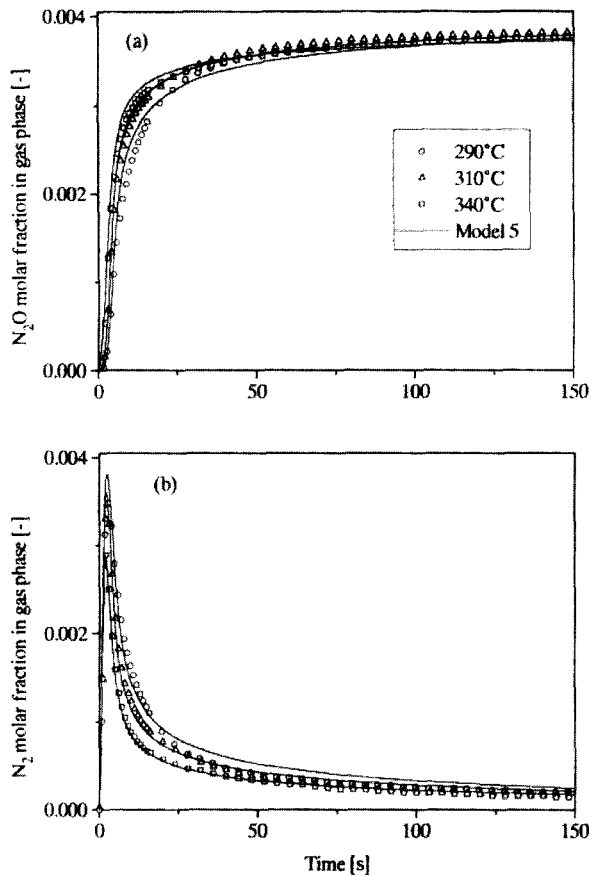


Fig. 5. Comparison between model 5 and experiment for a N₂O concentration step on a reduced catalyst at different temperatures. Conditions: $y_{N_2O,0}=0.004$, $Q=200 \text{ ml(NTP)/min}$ (runs 4–6). Some data points were omitted for clarity of the graph.

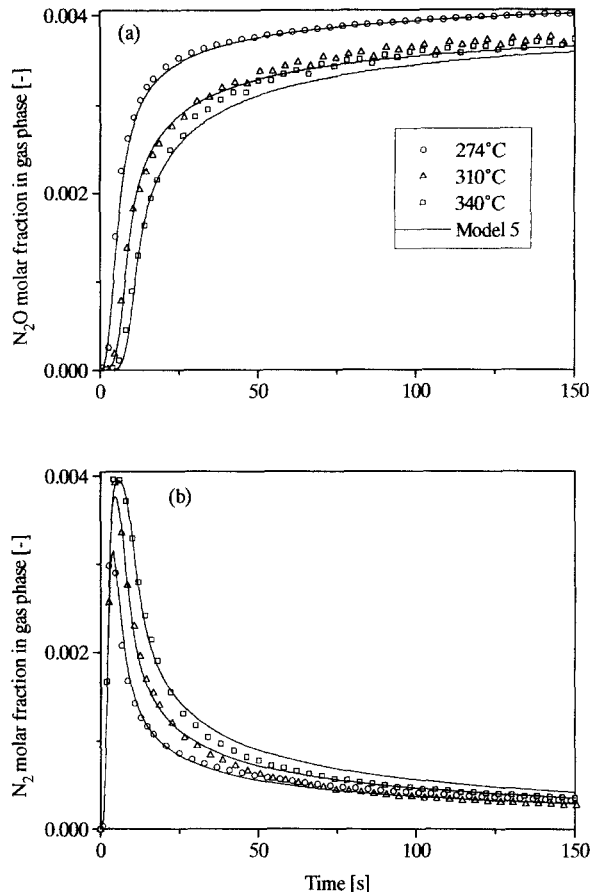
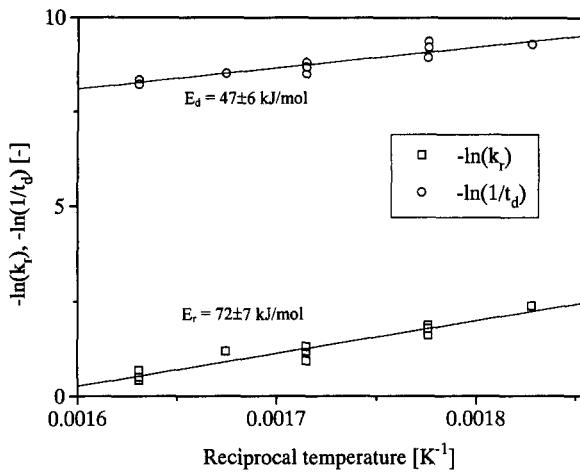
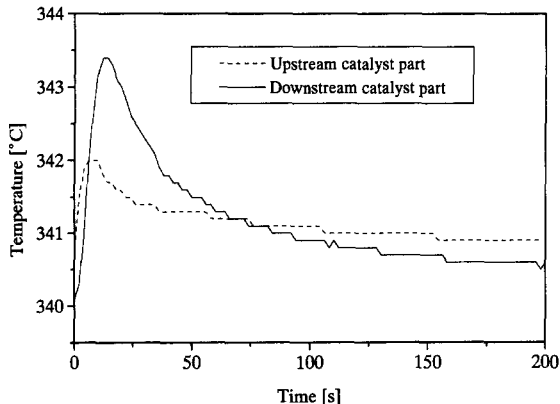


Fig. 6. Comparison between model 5 and experiment for a N₂O concentration step on a reduced catalyst at different temperatures. Conditions: $y_{N_2O,0}=0.004$, $Q=100 \text{ ml(NTP)/min}$ (runs 7, 9 and 11). Some data points were omitted for clarity of the graph.

4.2. Model 5: Effect of non-isothermicity

In general, the transient experiments presented in this work were accompanied by an initial rise in temperature of up to 4°C. This is illustrated in Fig. 8, where the temperature variation in time measured at upstream ($x\approx 0$) and downstream ($x\approx 1$) catalyst locations are shown for a N₂O concentration step with a molar fraction of 0.004 in the feed, an initial temperature (T_0) of 340°C and a total flow rate of 100 ml(NTP)/min (run 11). This run was chosen because it was carried out at high temperature, high residence time and at a high inlet molar fraction of N₂O. Under these conditions, the temperature rise is maximum. In order to check whether these temporal

temperature variations could significantly affect the transient responses – and thereby the estimated values of parameters – the transient response of the catalyst under non-isothermal conditions was simulated using model 5 (linear activity distribution combined with subsurface oxygen diffusion). This was done by integrating the temporal temperature profile measured at the downstream catalyst location ($x\approx 1$) to the model, and imposing an Arrhenius temperature dependence to the rate constant k_r and to the reverse characteristic diffusion time of oxygen in the iron oxide $1/t_d$ (Eqs. (21) and (22)). The initial values $k_r(T_0)$ and $1/t_d(T_0)$ were taken as the optimum values obtained during parameter optimisation. The activation energies for reaction and subsurface oxygen diffusion

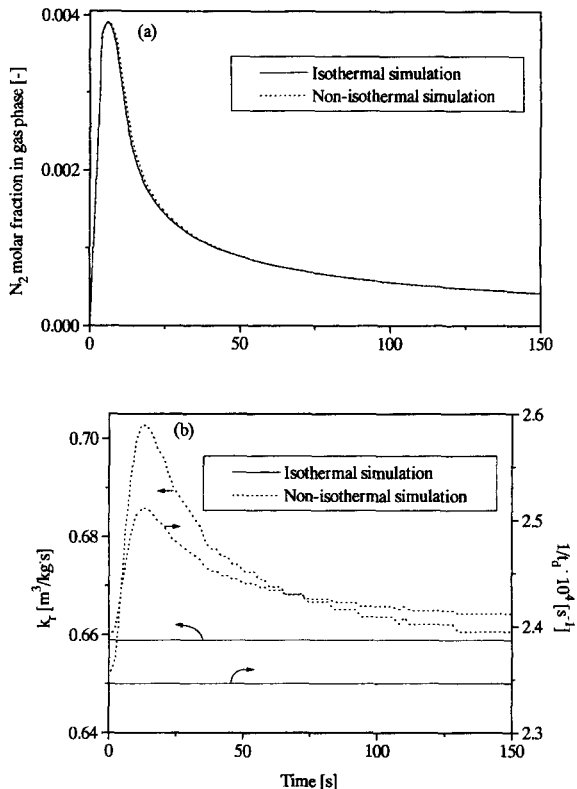
Fig. 7. Model 5: Arrhenius plot for k_r and $1/t_d$.Fig. 8. Temperature variation in time at upstream and downstream catalyst locations for a N_2O concentration step on a reduced catalyst. Conditions: $y_{\text{N}_2\text{O},0}=0.004$, $Q=100 \text{ ml(NTP)/min}$, $T=340^\circ\text{C}$ (run 11).

(respectively E_r and E_d) were taken as the values obtained from Arrhenius plots ($E_r=72 \text{ kJ/mol}$ and $E_d=47 \text{ kJ/mol}$).

$$k_r(T) = k_r(T_0) \exp \left[\frac{E_r}{R} \left(\frac{1}{T_0} - \frac{1}{T} \right) \right], \quad (21)$$

$$\frac{1}{t_d}(T) = \frac{1}{t_d}(T_0) \exp \left[\frac{E_d}{R} \left(\frac{1}{T_0} - \frac{1}{T} \right) \right] \quad (22)$$

In Fig. 9a, the non-isothermal response of N_2 is compared to the isothermal response. The corresponding variations of k_r and $1/t_d$ with time are shown

Fig. 9. Isothermal and non-isothermal responses of N_2 to a N_2O concentration step on a reduced catalyst. For the non-isothermal case: $E_r=72 \text{ kJ/mol}$ and $E_d=47 \text{ kJ/mol}$. In the lower graph: corresponding variations of k_r and $1/t_d$ with time. Curves are simulated with model 5. Conditions: $y_{\text{N}_2\text{O},0}=0.004$, $Q=100 \text{ ml(NTP)/min}$, $T=340^\circ\text{C}$ (run 11).

in Fig. 9b. The temperature rise leads to a maximum increase of the rate constant k_r of approximately 7.7% after 20 s, whereas the increase of $1/t_d$ is 6.8%. However, these changes in k_r and $1/t_d$ only slightly affect the transient response (Fig. 9a). Clearly, the similarity between curves shows that the temperature effect is negligible, even with a value for E_r as high as 72 kJ/mol.

5. Discussion

Firstly, it should be pointed out that the second-order reaction between gas phase N_2O and surface oxygen vacancies (model 1) totally fails to predict the

reaction under dynamic conditions, although it has been successfully used in previous works [5–8] to describe the N₂O reduction step during the reduction of NO with CO on Cu, Cr, Fe and Cu-rare earth oxide catalysts. With such a model, it is not possible to describe the sharp decrease of the rate of N₂ formation at the beginning of the transients together with the significant tailing of the transient responses. These characteristic features of the transient responses must arise from the combination of a fast initial surface reaction with another process with a longer relaxation time, such as a slow desorption, a phase transition or a diffusion-controlled process. The improvement of the fitting to the experimental data achieved by combining subsurface oxygen diffusion to the different rate equations (Eqs. (2),(4) and (9)) and the Arrhenius behaviour followed by the reverse characteristic diffusion time 1/t_d strongly suggest that oxygen diffusion becomes limiting at low degrees of reduction of the catalyst. The occurrence of subsurface oxygen diffusion in catalysis with metal oxides has been reported a number of times in recent literature, in particular during CO oxidation on Cu and Cr oxides [9–11], Bi–Mo oxides [12], MgO [13] and mixed oxides such as Fe–Sb–O or Bi–Mo–Fe–O [14]. During our measurements, the total amount of N₂ produced during N₂O step experiments on reduced catalysts was found to be equal to the amount of oxygen necessary to completely oxidise the catalyst from Fe₃O₄ to Fe₂O₃. This suggests that oxygen abstracted from N₂O at the surface can diffuse into subsurface oxygen vacancies. The reduction of the oxidised samples with CO produced the same amount of CO₂, indicating that the oxido-reduction cycles are reversible. As already mentioned in Section 1, pore diffusion resistance was considered negligible, since changing the diameter of the catalyst particles did not modify the tailing of the transient responses of N₂ and N₂O. The absence of pore diffusion effects is confirmed by the high value obtained for the activation energy of diffusion ($E_d=47$ kJ/mol). Such a value for an activation energy of diffusion is rather characteristic of a diffusion process in the bulk of the iron oxide. However, the values reported in literature for the activation energies of diffusion of oxygen or iron in magnetite are higher than the value determined in the present study. For instance, Castle and Surman [15] have reported a value of 71 kJ/mol for the activation energy

of diffusion of oxygen in Fe₃O₄, whereas a value of 109 kJ/mol was measured by Heizmann et al. [16]. A value of 89.9 kJ/mol for the activation energy of diffusion of iron ions in magnetite has been reported by Gillot [17]. The lower value obtained for E_d in our case in comparison to the values found in literature for diffusion in magnetite could be due to the fact that oxygen formed at the surface via N₂O reduction has to diffuse through a mixed layer of magnetite and hematite, with a lower resistance to oxygen transfer by diffusion as for pure magnetite.

The use, in model 5, of a linear activity distribution leads to a second-order reaction with respect to surface oxygen vacancies (Eq. (4)). The assumption of a linear activity distribution is in agreement with Mössbauer spectroscopic investigations of the interaction between N₂O and iron oxide [18], which showed that the reduction of N₂O is second order with respect to Fe²⁺ ions. Furthermore, during the reduction of N₂O, the catalyst (initially Fe₃O₄) is oxidised to Fe₂O₃ [19]. This process is accompanied by a structural change from the cubic magnetite lattice to the hexagonal oxygen lattice of hematite, which could be the origin of the linear decay of the rate constant with the degree of reduction of the surface.

6. Nomenclature

<i>Bo</i>	Bodenstein number
<i>c</i> _{N₂}	gas phase concentration of N ₂ , mol/m ³
<i>c</i> _{N₂O}	gas phase concentration of N ₂ O, mol/m ³
<i>c</i> _{N₂O,0} (<i>t</i>)	N ₂ O inlet concentration step function, mol/m ³
<i>c</i> _(O)	oxygen vacancy concentration in the catalyst, mol/kg _{cat}
<i>c</i> _(O)	oxygen concentration in the catalyst, mol/kg _{cat}
<i>D</i>	diffusion coefficient of oxygen in iron oxide, m ² /s
<i>d</i> _p	diameter of particles, m
<i>E</i> _d	activation energy for subsurface oxygen diffusion, kJ/mol
<i>E</i> _r	activation energy for surface reaction, kJ/mol
<i>k</i>	rate constant, m ³ /kg _{cat} s
<i>k</i> _r	rate constant for the reduced catalyst, m ³ /kg _{cat} s

k_{r0}	pre-exponential factor, $\text{m}^3/\text{kg}_{\text{cat}} \text{s}$
L	catalyst bed length=0.01 m
m_{cat}	amount of catalyst, kg
N_s	total concentration of sites=0.33 mol/ kg_{cat}
NTP	normal conditions of temperature and pressure (0°C , $1.013 \times 10^5 \text{ Pa}$)
p	pressure in the reactor, kPa
Pe_{ax}	axial Peclet number
Q	total volumetric flow rate, $\text{ml}(\text{NTP})/\text{min}$
r	surface reaction rate, $\text{mol}/\text{kg}_{\text{cat}} \text{s}$
R_{N_2}	N_2 rate of formation, $\text{mol}/\text{kg}_{\text{cat}} \text{s}$
$R_{\text{N}_2\text{O}}$	N_2O rate of disappearance, $\text{mol}/\text{kg}_{\text{cat}} \text{s}$
R_ϕ	rate of disappearance of surface oxygen vacancies, $\text{mol}/\text{kg}_{\text{cat}} \text{s}$
R	gas constant, kJ/mol K
t	time, s
t_d	characteristic diffusion time, s
t_{d0}	characteristic diffusion time at infinite temperature, s
T	temperature, K
x'	distance from the reactor inlet, m
$x=x'/L$	dimensionless distance from the reactor inlet
y	molar fraction
y_{N_2}	N_2 molar fraction
$y_{\text{N}_2\text{O}}$	N_2O molar fraction
$y_{\text{N}_2\text{O},0}$	N_2O molar fraction in feed
$y_{\text{N}_2\text{O},0}(t)$	N_2O inlet step function
z'	distance from the centre of the spherical-geometry iron oxide crystallite, m
$z=z'/\delta$	dimensionless distance from the centre of the spherical-geometry iron oxide crystallite
()	oxygen vacancy
(O)	oxygen species

Greek letters

α	exponential activity distribution parameter
β	exponential activity distribution parameter
δ	thickness of the iron oxide layer, m
ϵ_b	void fraction of catalyst=0.5
ϕ	degree of reduction of the catalyst
ρ_{cat}	catalyst bulk density=373.5 kg/m ³
τ	space time, s

Subscripts

0	inlet
j	index for gas phase species (N_2 , N_2O)
s	index for the surface

Acknowledgements

The authors acknowledge support from the Swiss National Science Foundation.

References

- [1] H. Randall, R. Doepper and A. Renken, Can. J. Chem. Eng., 74 (1996) 586–593.
- [2] M. Baerns, H. Hofmann, A. Renken, Lehrbuch der Technischen Chemie-Band 1, Chemische Reaktionstechnik, 2nd ed., Georg Tieme Verlag, Stuttgart, 1992, p. 342.
- [3] J.J. Carberry, Chemical and Catalytic Reaction Engineering, McGraw-Hill, New York, NY, 1976, p. 379.
- [4] Simusolv®, Modeling and Simulation Software, Reference Guide, Dow Chemical Company, Midland, MI, 1990.
- [5] Y. Jacquier, Diploma Thesis, Ecole Polytechnique Fédérale, Lausanne, 1995.
- [6] G.V. Glazneva, A.A. Davidov, I.S. Sazonova, Y.M. Shchekochikhin and N.P. Keier, React. Kinet. Catal. Lett., 9 (1978) 131–136.
- [7] N. Yoneda, S. Ito and H. Yamagishi, J. Jpn. Soc. Air Pollut., 16 (1981) 88–93.
- [8] E. Echigoya, J. Jpn. Petrol. Inst., 23 (1980) 223–232.
- [9] F.H.M. Dekker, Ph.D. Thesis, Department of Chemical Engineering, Faculty of Chemistry, University of Amsterdam, Amsterdam, 1995.
- [10] C.M.A.M. Mesters, A. De Koster and O.L.J. Gijzeman, Appl. Surf. Sci., 20 (1984) 1.
- [11] O.P. Van Praussen, M.M.M. Dings and O.L.J. Gijzeman, Surf. Sci., 179 (1987) 377–386.
- [12] R.K. Grasselli, J.D. Burrington and J.F. Brazdil, Faraday Discuss. Chem. Soc., 72 (1982) 203.
- [13] O.Yu. Ovsitser, K.S. Guljaev and V.D. Sokolovskii, Catal. Lett., 20 (1984) 1–12.
- [14] O.Yu. Ovsitser and V.D. Sokolovskii, Catal. Lett., 17 (1993) 239–244.
- [15] J.E. Castle and P.L. Surman, J. Phys. Chem., 73 (1969) 632–634.
- [16] J.J. Heizmann, P. Becker and R. Baro, Membr. Sci. Rev. Met., 70 (1973) 625–636.
- [17] B. Gillot, Ann. Chim., 6 (1981) 591–604.
- [18] V.I. Yaskevich, G.N. Kotova and G.K. Alekseeva, Kinet. Katal., 31 (1990) 1003–1007.
- [19] I. Guyette, Diploma Thesis, Université Catholique de Louvain, Louvain-La-Neuve, 1994.